SEABED SCATTERING CROSS SECTION ESTIMATION USING THE RESON SEABAT T50: A NUMERICAL EVALUATION OF THE FOOTPRINT ERROR WHEN USING A ZERO-SLOPE ASSUMPTION IN THE ALONG-TRACK DIRECTION

Gorm Wendelboe

Teledyne RESON

Contact author: Gorm.Wendelboe@Teledyne.com, Teledyne RESON A/S, Fabriksvangen 13, 3550 Slangerup, Denmark. Phone +45 4738 0022.

Abstract: *The bottom scattering cross section estimated by the RESON SeaBat T50 multibeam echosounder (MBES) includes an estimate of the insonified area, which is obtained by assuming the seabed has a vanishing slope in the along-track direction. In this paper, the validity of this assumption is investigated for different along-track slopes, depths, and continuous wave (CW) pulse durations using a numerical model. It is demonstrated how the errors are largest around normal incidence and rapidly decrease as steering angle increases. The errors can be reduced by increasing the CW pulse duration. For example, at 400kHz, a 40μs CW pulse transmitted over a nadir-depth of 35m will, for seafloors with along-track slopes of 5% and 15%, yield errors of 1.5 and 5dB, respectively. If, however, the duration of the CW pulse is increased to 100μs, the resulting errors are reduced to 0.05 and 1.5dB, respectively. Finally, a brief description is given of how the estimated footprint areas can be removed from the estimated scattering cross section values and replaced by the user's own estimates.*

Keywords: *multibeam echosounder, seabed scattering strength, insonified area.*

1. INTRODUCTION

Over the recent decades, various acoustic measurements have shown that the seabed back-scattering strength S_b obtained at frequencies between 20-500kHz depends on whether the seabed consists of sand, gravel, mud, rock, gravel, or a mixture of those [1]-[6]. Species present on top of or inside the sediment may also have an influence on S_b [7]. The scattering strength varies with the angle of incidence and it may vary with the acoustic frequency depending on sediment type. The scattering strength is a physical property of the seabed, and the acquisition of S_b requires a calibrated sonar [8]. The SeaBat T50 multibeam echosounder (MBES) provides estimates of the seabed scattering strength [6]. The estimates of the insonified area are based on the assumption that the seabed has zero slope in the along-track direction, which may lead to incorrect S_b-estimates. Here, the validity of the assumption is assessed using a numerical model, in which the MBES beam patterns are projected on a seafloor plane, and where the footprint area will be calculated as the convolution of the transmitted tone-burst with the seafloor as a function of time. The approach is particularly important close to nadir [9][10]. Along-track slopes between 2% -15% (≈ 1° - 9°) are considered.

2. A 3D NUMERICAL MODEL OF THE INSONIFIED AREA

The model will consider an MBES transmitting a continuous waveform (CW) pulse, also known as a tone-burst, of duration τ with carrier frequency $f_c = 400$kHz onto a plane and horizontal seabed.
Figure 1(a) shows the applied coordinate system. The x-axis is pointing in the across-track direction, the y-axis in the along-track direction, and the z-axis upwards. The origin is located at the center of the receiver (Rx), and with zero pitch angle, i.e., $\alpha = 0$, the center of the transmitter (Tx) is located at $\vec{r}_{Tx}(0) = [0\ y_{Tx}\ 0]^T$. Roll, heave, and heading are not included. A point on the seafloor is given by the vector $\vec{r} = \begin{bmatrix} r_x & r_y & -H \end{bmatrix}^T$, where H is the depth.

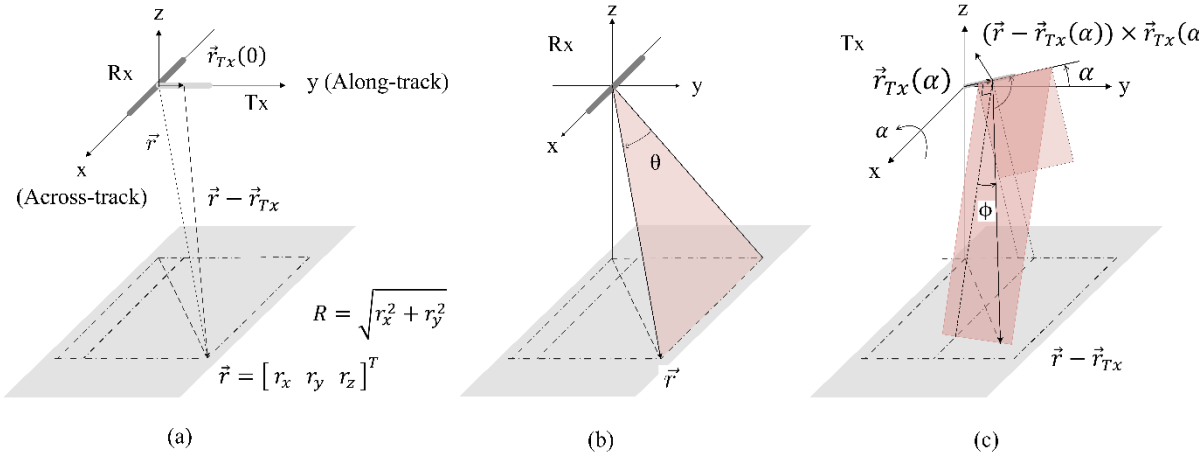

Figure 1: Geometry applied (a), the angle θ used for the Rx beamformer beam pattern (b), and the angle ϕ used for the Tx beam pattern (c).

The Tx sensitivity is assumed constant in the across-track direction between -65° and 65°, and the Rx sensitivity is assumed constant in the along-track direction between -20° and 20°. Thus, Tx and Rx are represented as line arrays, i.e., the arrays that are rotationally symmetric around their main axes. The beam patterns of interest are the beamformed Rx beam pattern in the

across-track direction, with a 3dB beam width of approximately 0.5°/cos(θ_s), where θ_s is the steering angle, and the Tx beam pattern in the along-track direction with a 3dB opening angle of 1°. The purpose is to project the beam patterns onto discrete points on the seabed. The far-field beamformed Rx beam pattern b_{Rx} is obtained by the following expression [11]:

$$b_{Rx} = \sum_{n=1}^{N_0} w_n e^{-iknd(\sin(\theta)-\sin(\theta_s))} \tag{1}$$

where $N_0 = 256$ is the number of channels, and w_n is the energy-normalized shading coefficient for the n'th channel; here the receiver shading is a Chebyshev window with a sidelobe suppression magnitude factor of 30dB. Next, in Eq. (1) i is the imaginary number, $k = 2\pi f_c/c$ is the wave number obtained with a speed of sound $c = 1500$ m/s, $d = 1.6$mm is the sensor spacing. Finally, θ_s is the steering angle, and θ is the angle of the incoming field from the point $\vec{r}$, where $\sin(\theta) = r_x/|\vec{r}|$, see, e.g., Figure 1(b). For any given point on the seabed the corresponding b_{Rx} value is obtained using Eq. (1). An example of the receiver beam pattern for a steering angle of 20° is shown in Figure 2 (left).
The far-field beam pattern of the transmitter in the along-track direction b_{Tx} is obtained from a look-up table with values populated by a company proprietary model. b_{Tx} is shown in Figure 2 (right). An along-track sloping seafloor is simulated by rotating the transmit array around the x-axis by the angle α. The along-track transmit beam angle ϕ is equal to zero at the center of the Tx along-track beam, and for any point on the horizontal seabed plane it is computed from the cross-product between the vector from the Tx center to the seabed point and the vector from the origin to the Tx center, i.e.,

$$\phi = \frac{\pi}{2} - \sin^{-1}\left(\frac{\left|\left(\vec{r} - \vec{r}_{Tx}(\alpha)\right) \times \vec{r}_{Tx}(\alpha)\right|}{|\vec{r} - \vec{r}_{Tx}(\alpha)|\,|\vec{r}_{Tx}(\alpha)|}\right) \tag{2}$$

see, e.g., Figure 1(c).

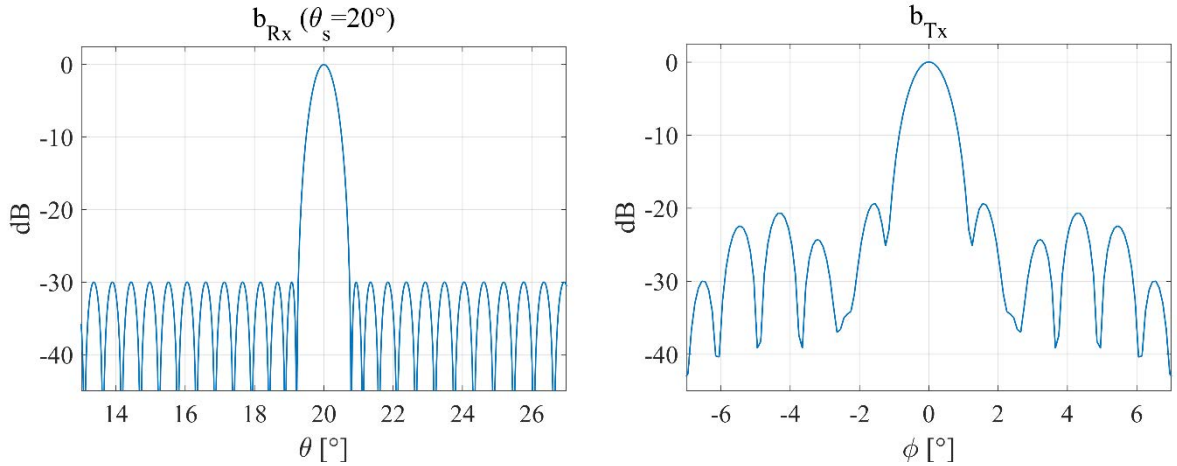

Figure 2: Across-track beam pattern of the Rx beam former (left) Along-track Tx beam pattern (right) both at 400 kHz.

The integration area is reduced to a region around the point where the center beam of the transmitter crosses the center of the steered beam on the seabed. For illustrative purposes, the area covers what corresponds to $\pm 5\theta_{3dB}$ in the across-track direction and $\pm 5\phi_{3dB}$ in the along-track direction.

Close to nadir, the seabed plane is divided into rectangular grids with a size governed by the width of the main beams. The angular resolution is $\Delta\theta = \theta_{3dB}/30 = 0.5°/30$, and the resolution in the across-track direction yields

$$\Delta x = H\,[\tan(\theta_s - \theta_{3dB} + \Delta\theta) - \tan(\theta_s - \theta_{3dB})] \tag{3}$$

Equivalently, $\Delta\phi = \phi_{3dB}/60 = 1°/60$, and the resolution in the along-track direction, Δy, is obtained by replacing θ_{3dB} with ϕ_{3dB} and setting $\theta_s = 0$ in Eq. (3). The instantaneous footprint area is obtained as the product of the projected Tx and Rx beam pattern squared and integrated over the tone-burst projected area on the seabed at a given point in time (see, e.g., Eq. G.4, p. 495, [5]). Using the seabed model, the insonified area is expressed as

$$A(n, \theta_s, H) = \Delta x\,\Delta y \sum \left\{ b_{Tx}^2(x_i, y_j)\; b_{Rx}^2(x_i, y_j; \theta_s) \middle| R_1 \le \sqrt{x_i^2 + y_j^2} \le R_2 \right\} \tag{4}$$

where n is the sample number, i and j are indices of the discrete x - and y points respectively, and

$$R_1 = \left\{ \sqrt{\left(n\Delta r_{T_s} - \Delta r_\tau\right)^2 - H^2} \;\middle|\; n \ge (H + \Delta r_\tau)/\Delta r_{T_s} \right\} \tag{5}$$

(otherwise $R_1 = 0$), that is, the ground range distance from the origin to the rear edge of the pulse on the seabed plane (see, e.g., Figure 1(a)); $\Delta r_{T_s} = c\,T_s/2$ is the sampling range resolution, and T_s is the sampling time; $\Delta r_\tau = c\tau/2$ is the physical range resolution, and τ is the tone-burst duration. Finally, in Eq. (4), R_2 is the front edge of the pulse on the seabed, and it is given by

$$R_2 = \left\{ \sqrt{\left(n\Delta r_{T_s}\right)^2 - H^2} \;\middle|\; n \ge H/\Delta r_{T_s} \right\} \tag{6}$$

(otherwise $R_2 = 0$). For simplicity, the offset y_{Tx} is not included in Eqs. (4)-(6); the impact of this approximation is considered to induce insignificant offsets of the integration areas. Cartesian coordinates are applied up to an angle, which corresponds to the maximum disk size multiplied by a factor ν, i.e.,

$$\theta_T = \nu \cos^{-1}\left(\frac{H}{H + \Delta r_\tau}\right) \tag{7}$$

where $\nu = 5$ is applied. For $\theta_s > \theta_T$, integration is carried out using polar coordinates so that

$$A(n, \theta_s, H) = R_n\,\Delta R_n\,\Delta\alpha \sum_{m=1}^{M} b_{Tx}^2(n, j)\; b_{Rx}^2(n, j; \theta_s) \tag{8}$$

where n is the sample number, $R_n = \sqrt{r_n^2 - H^2}$ is the ground range, $\Delta R(n, \theta_s) = \Delta r_\tau / \cos(\theta_g)$ is the pulse projected on the seafloor, $m = 1,2,..,M$ is the index of an angular sub-sector out of M sectors. Each sector has a radial resolution of $\Delta\alpha = \Delta\phi_{3dB}/30$ =1°/30. The beam patterns are projected onto the seabed points with coordinates$(R(n)\cos(\alpha_m), R(n)\sin(\alpha_m))$.

3. SIMULATION RESULTS

All simulations have been made with $f_c = 400$kHz. The along-track seabed slopes are presented as linear percentage slopes. For example, a slope of 10% corresponds to a bottom that changes the depth by 10m over a distance of 100m. The distance between the origin and the center of the Tx is set to y_{Tx} = 0.25m. The sampling time used in the simulations is T_s = 5.76μs.

Figure 3(a-c) shows the time progression of the footprint area for the beam with steering angle θ_s = 2°. Figure 3(d) shows total area as a function of time. The duration of the tone-burst is τ = 40μs, and the depth is H=35m. Three instances in time after the front side of the signal has reached the seabed are shown. At time t_1= 20μs (a) the footprint area is a small disk containing the main lobe of the combined 2D beam pattern; the total area is approximately 20dB below the maximum value (d). At time t_2 = 56μs the insonified area is an annulus (b), and where the insonified area includes the main lobe of the combined beam pattern, and the total area has reached the maximum of -6.5dB re 1 (d). At t_3 = 80μs the annulus is moving out of the main lobe of the combined beam pattern, and the total area has, at this point in time, already been reduced by approximately 10dB since time t_2 (d). The blue dotted line in Figure 3(d) represents the total area obtained with the 3D numerical model presented in the previous section. The red dotted line is the total area produced by the 2.5D algorithm applied for the SeaBat T50; a model that does not include side-lobes.

Figure 4 shows the maximum insonified area as a function of beam angle for six different along-track slopes at a depth of 35m. Figure 4(a) shows for the case where the tone-burst has a duration of τ = 40μs: At the nadir beam a 5% sloping bottom yields an error of 1.5dB when compared to the bottom with 0% slope; at 7% the error is about 2.5dB, and at 15% it is about 5dB. As the steering angle increases the errors decrease and become insignificant above θ_s = 35°. Figure 4(b) shows the results for a similar investigation, but with τ = 100 μs: A 5% sloping bottom does not produce an error at the nadir beam; a 7% sloping bottom only yields an insignificant error of about 0.1dB, and at 15º it is about 1.7dB. Thus, by increasing the duration of the tone-burst the error will decrease.

Figure 5 shows the relative error of the maximum footprint area at nadir as a function of depth. Figure 5(a) shows the error for a tone-burst duration of τ = 40μs: If the error must be less than 1dB, then at 30m and 50m the slope is allowed to be up to 5% and 3%, respectively. Figure 5(b) shows the errors when τ = 100μs: If the error must be less than 1dB, then at 30m and 50m the slope is allowed to be up to 11% and 7%, respectively.

Figure 6 shows the relative error of the maximum footprint at nadir as a function of tone-burst duration. Figure 6(a) shows the expected errors at a depth of 20m. If τ>120μs the errors will be negligible even for slopes up to 15%. Figure 6(b) shows the expected footprint errors at a depth of 35m; if τ>120μs the errors will be negligible for slopes up to 7%.

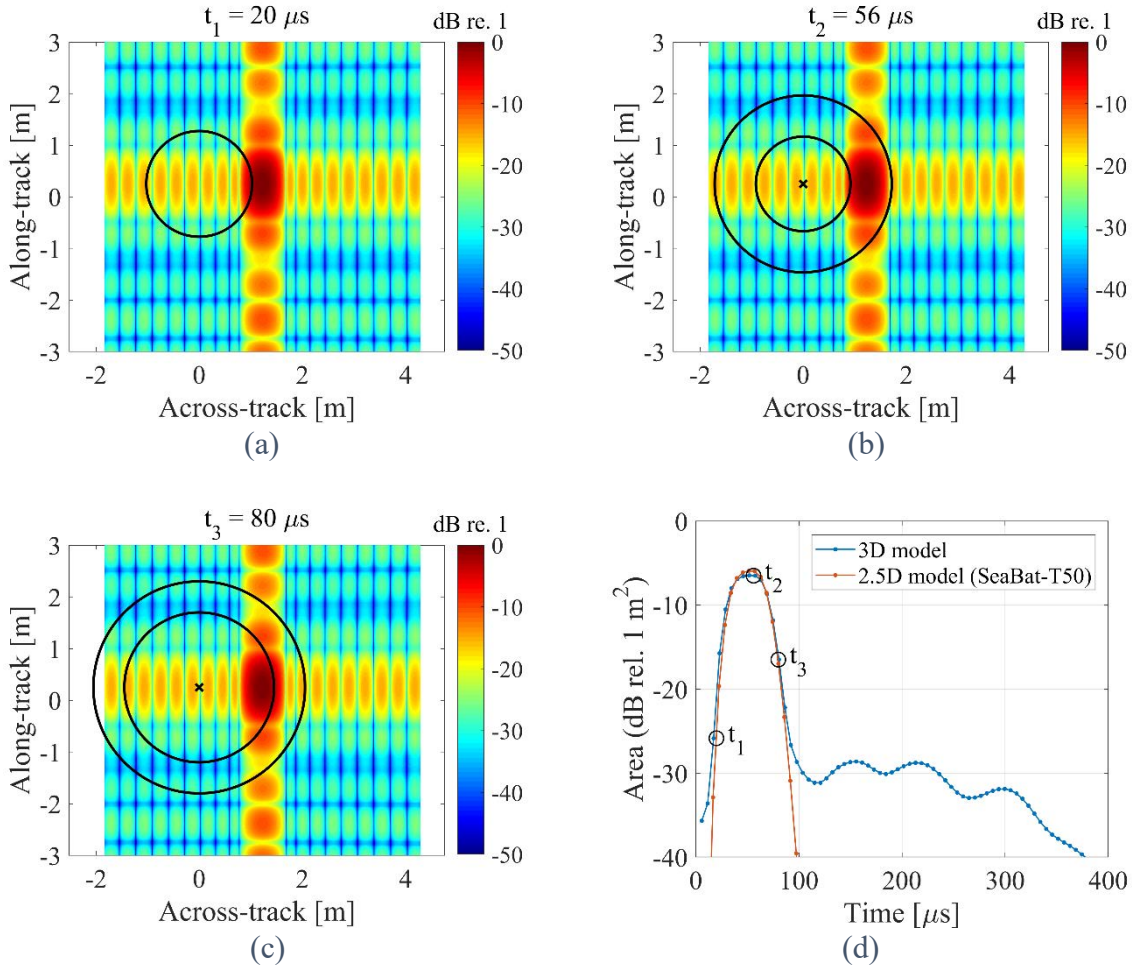

Figure 3: Time evolvement of the footprint area at θ_s = 2° on a non-sloping seabed. The tone-burst center frequency is f_c =400kHz, τ =40μs, and H =35m. Figures 1(a)-1(c) show the insonified area at three different points in time after the front side of the pulse has reached the seabed. Finally, Figure 1(d) shows the footprint area as a function of time.

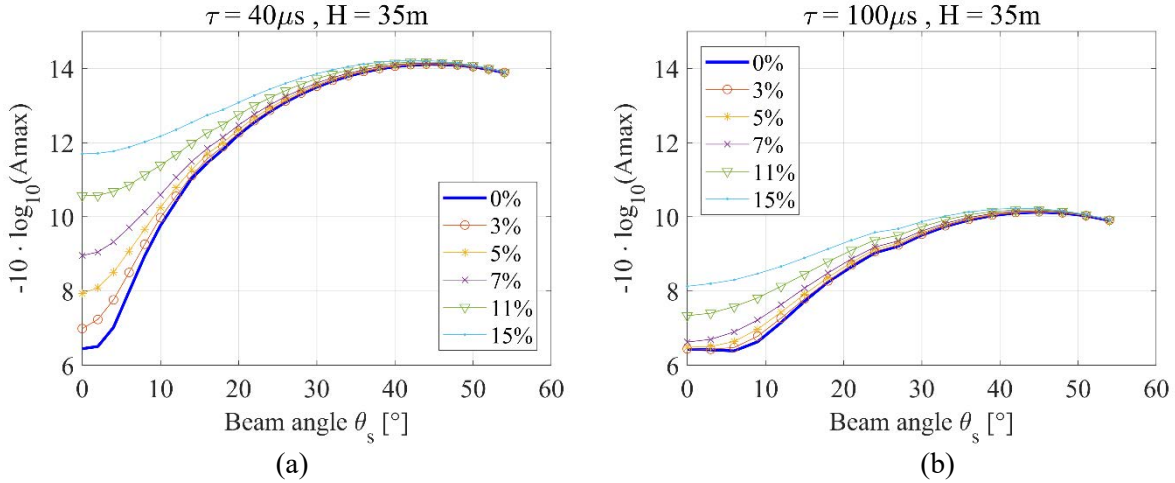

Figure 4: The maximum insonified area as a function of beam angle for six different seabed slopes in the along-track direction

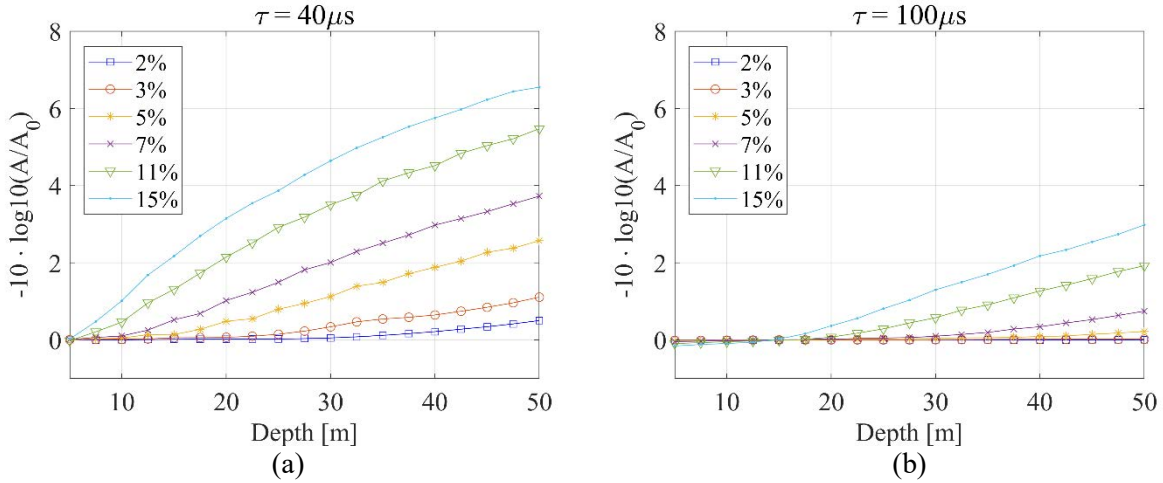

Figure 5: Relative error of the maximum insonified area within the nadir beam as a function of depth. The reference area A_0 is the area of a non-sloping seafloor.

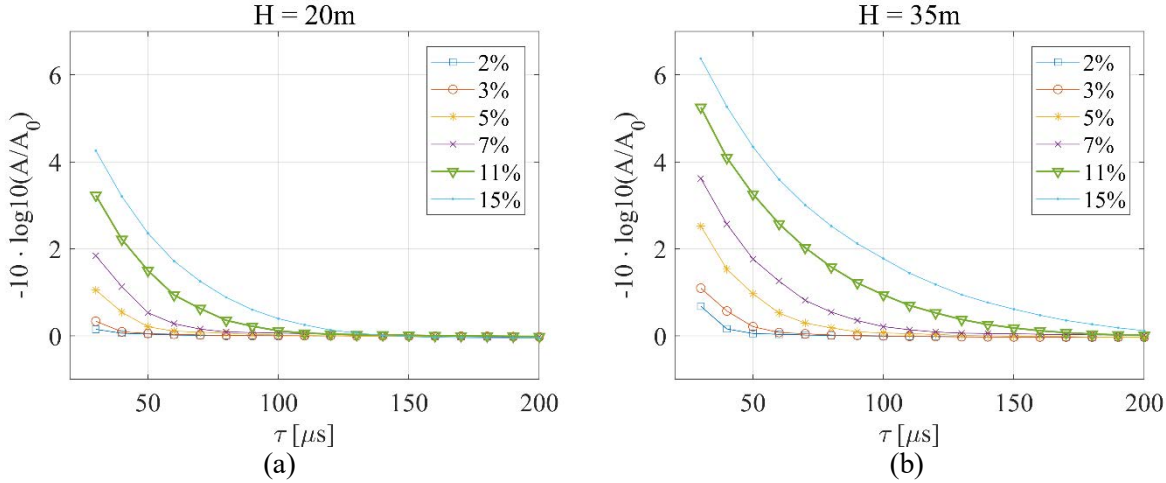

Figure 6: Relative error of the maximum insonified area within the nadir beam as a function of tone-burst duration. The reference area A_0 is the area of a non-sloping seafloor.

4. PROCESSING OPTION FOR THE MBES USER

For each S_b -value stored in the T50 datagram (Record 7058) [12] the associated footprint area value A_{T50} is also stored. It is possible to replace A_{T50} with an alternative footprint value, for instance based on a 3D bottom geometry produced by survey software packages such as QPS™ or Teledyne CARIS™. The scattering cross section is obtained from the scattering strength by $\sigma = 10^{(S_b/10)}$, where $\sigma = K_{T50}/A_{T50}$, and where K_{T50} is a factor that depends on environmental conditions and other MBES parameters. The modified scattering cross section can be obtained by

$$\sigma_m = \sigma A_{T50}/A_m \tag{9}$$

where A_m is the alternative footprint area. The grazing angle, i.e., the angle between incoming field and the seabed surface, is not included in the datagram, but it is crucial for further analysis. Thus, if the σ -values obtained from the T50 datagram are selected for analysis, the grazing angle can be obtained from the datagram that includes the bottom detection points (Record 7027), and from which the height profile obtained from a ping can be used to estimate the grazing angles.

5. SUMMARY

The algorithm, which estimates S_b for SeaBat T50 data, neglects the slope of the seabed in the along-track direction. Consequently, surveys over areas with high topographic variations or depth gradients in the along-track direction may lead to flawed S_b-estimates. The errors are dominant near normal incidence, and they will decrease with increasing angle of incidence at the outer beams. The errors increase with increasing along-track gradients and with depth. However, if the duration of the transmitted CW pulse is increased the errors are reduced significantly. Thus, for best possible backscatter performance is it recommended to use CW pulses with durations between 80-200µs depending on the depth and the seabed topography. Alternatively, it is possible for the user to replace the footprint values with the user's own estimates.

REFERENCES

[1] **C.M. McKinney, C.D. Anderson**, Measurements of backscattering of sound from the ocean bottom, *J. Acoust. Soc. Am.*, 36 (1), pp. 158-163, 1964.

[2] **P.D. Mourad, D.R. Jackson, A**, High frequency sonar models for bottom backscatter and forward loss, In *Proc. OCEANS*, pp. 1168-1175, 1989.

[3] **D.G. Simons, M. Snellen**, High frequency measurements of bottom backscattering strength in the North Sea: Correlation with grain size, shell content and gravel content, In *Boundary Influences in High Frequency, Shallow Water Acoustics,* University of Bath, pp. 177-184, 2005.

[4] **T.C. Weber, L.G. Ward**, Observations of backscatter from sand and gravel seafloors between 170 and 250 kHz, *J. Acoust. Soc. Am.*, 138 (4), pp. 2169-2180, 2015.

[5] **D.R. Jackson, M.D. Richardson**, *High-Frequency Seafloor Acoustics*, Springer, 2007.

[6] **G. Wendelboe**, Backscattering from a sandy seabed measured by a calibrated multibeam echosounder in the 190–400 kHz frequency range, *Marine Geophysical Research*, 39 (1-2), pp. 105-120, 2018.

[7] **M.S. Ballard, K.M. Lee**, The acoustics of marine sediments, *Acoustics Today*, 13 (3), pp. 11-18, 2017.

[8] **G. Larmarche, X. Lurton**, Introduction to the Special Issue "Seafloor backscatter data from swath mapping echosounders: from technological development to novel applications", *Marine Geophysical Research*, 39 (1-2), pp. 1-3, 2018.

[9] **D. Jackson, B.T. Hefner, A. Ivakin, G. Wendelboe**, Seafloor characterisation using physics-based inversion of multibeam sonar data, In *Proc. 11th European Conference on Underwater Acoustics (ECUA 2012)*, Edinburgh, pp. 258-263, 2012.

[10] **L. Bjørnø**, *Applied Underwater Acoustics*, T.H. Neighbors and D. Bradley, Elsevier, pp. 532-535, 2017.

[11] **P. S. Naidu**, *Sensor array signal processing*, CRC Press, Elsevier, pp. 75-94, 2001.

[12] **Teledyne-RESON**, Data Format Definition Document. 7k Data Format, https://www.teledyne-pds.com/faq-2/where-can-i-find-the-latest-teledyne-reson-7k-dfd/